Active anti-sway crane control using partial state feedback from inertial sensor

Václav Helma*, Martin Goubej†
NTIS Research Centre, Faculty of Applied Sciences
University of West Bohemia
Pilsen, Czechia
Email: *helma@ntis.zcu.cz, †mgoubej@ntis.zcu.cz

***Abstract*—The paper deals with development of active anti-sway feedback control method for gantry cranes. Inertial measurement unit is chosen as a load motion sensing device allowing to close a feedback loop. The paper provides guidelines for the successive steps of mathematical modelling, data-driven identification and model-based controller design. The proposed method is experimentally validated on an industrial overhead crane system.**

I. Introduction

Crane systems are considered to be a most common type of manipulators used in numerous pick-and-place applications ranging from construction to factory automation or offshore cargo handling. Crane operators have to deal with inherently underactuated dynamics of the hanging load causing unwanted transient and residual oscillations.

Extensive research has been devoted to development of various anti-sway control systems in recent years to aid the human operators with precise, safe and reliable manipulation. The developed solutions can be roughly divided into two main categories. Passive approaches try to modify the motion trajectories of the crane in a feedforward manner to avoid excitation of the load resonance frequencies. Various types of notch, smoothing or zero vibration input shaping filters can be used for this purpose [1]–[5]. Main advantage of the feedforward approaches is the simplicity of implementation. On the other hand, moderate robustness to uncertainty and impossibility to compensate for external disturbance are considered to be main drawbacks. Active approaches employ a sensing device which detects position of the hanging load and close a feedback loop. In this manner, both vibrations due to reference and external disturbances can be attenuated.

Various strategies have been proposed for the design of the feedback controller [6]–[9] using several ways of obtaining the load motion feedback ranging from cameras supplemented by advanced image processing algorithms [10]–[14] through lasers [15] or inclinometers [16] to the utilization of IMUs [17] (inertial measurement units). Particularly the use of IMUs combining the accelerometers and angular rate sensors (known also as gyroscopes) seems to be appealing due to low acquisition cost and small dimensions of the device. Moreover, the IMU can be easily mounted to the load-side of the crane. The proper spot to place the unit is probably the crane hook as it allows an easy installation of the sensor and, unlike the IMU location on the carried load itself, it does not require the reattachment of the unit whenever the load is replaced. Therefore, we opted for development of IMU-based feedback solution to active anti-sway system.

A particular difficulty encountered when dealing with feedback control of cranes comes from their oscillatory dynamics containing multiple resonance modes. Majority of the methods proposed in the literature use a simplified single pendulum on cart model [9]. It may serve as a reasonable approximation of the most dominant low-frequency mode of the hanging load and usually proves to be sufficient for the design of feedforward controllers. However, employing feedback methods using overly simplified models often leads to problems with unmodelled dynamics. Especially weakly damped mechanical systems are prone to spill-over effect which may cause closed-loop instability due to the occurrence of unmodelled higher bending modes [18]. Crane systems with non-negligible hook mass and length of the thimble used for the load attachment typically exhibit second significant mode of oscillations. For this sake, double-pendulum model may be more relevant for active stabilization. Combining the aforementioned IMU-based sensing system with the double-pendulum dynamics forms a control scenario with a partially available state information, as only hook motions are directly measured. This requires careful design of the feedback controller. This paper presents a suitable approach which is experimentally validated using an industrial grade crane system.

The paper is organized as follows. Section II derives the mathematical model of the double-pendulum system and explains the functionality of the load motion sensor. Combination of the assumed model structure and data-driven experimental identification is used to acquire a plant model that is subsequently used to design a feedback controller providing the desired active anti-sway functionality. Section III deals with experimental validation of the proposed control strategy using a five ton industrial overhead crane.

II. Algorithms and methods

A. Physical analysis of the system

The gantry crane can be modelled as a double-link pendulum on the cart (see Fig. 1). The first link then represents the hook suspended by rope from the hoist while the second one is a load hanging on the hook. First, we will use the Lagrange's equations to derive the model of the general n-link pendulum

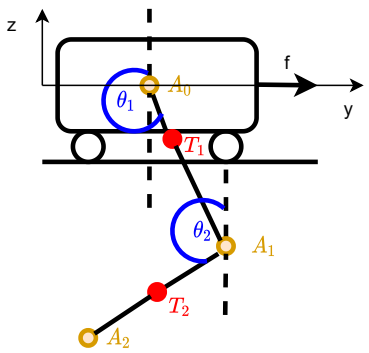

Fig. 1. Double pendulum on cart with $A_{\{0,1,2\}}$ denoting axes of rotation, $T_{\{1,2\}}$ designating the centers of gravity and $\varphi_{\{1,2\}}$ the deflection angles

on cart (for details see [19]). For this purpose, we need to state the relationships for the potential and kinetic energy

$$V(t) = \sum_{k=1}^{n} m_k g Z_k(t), \tag{1}$$

$$T(t) = \sum_{k=1}^{n} \left\{ \frac{1}{2} m_k \left[\left(\frac{dY_k(t)}{dt} \right)^2 + \left(\frac{dZ_k(t)}{dt} \right)^2 \right] + \frac{1}{2} J_k \left(\frac{d\theta_k(t)}{dt} \right)^2 + \frac{1}{2} m_0 \left(\frac{dy_0(t)}{dt} \right)^2 \right. \tag{2}$$

where the particular points can be expressed as

$$y_i(t) = \sum_{k=1}^{i} l_k sin(\theta_k(t)) + y_0(t), \quad z_i(t) = \sum_{k=1}^{i} l_k cos(\theta_k(t)), \tag{3}$$

$$Y_i(t) = \sum_{k=1}^{i-1} l_k sin(\theta_k(t)) + a_i l_i sin(\theta_k(t)) + y_0(t), \tag{4}$$

$$Z_i(t) = \sum_{k=1}^{i-1} l_k cos(\theta_k(t)) + a_i l_i cos(\theta_k(t)). \tag{5}$$

Here, $A_0, \dots A_{n-1}$ are the revolute joints and A_n the free end of the pendulum. These points are characterized by coordinates as $A_i(t) = [y_i(t), z_i(t)]^T$. We will also denote $T_0(t), \dots, T_n(t)$ ($T_i(t) = [Y_i(t), Z_i(t)]^T$) the centre of gravity of the pendulum links, $\theta_0(t), \dots, \theta_n(t)$ the pendulum link angles with respect to the axis of rotation. Further, m_i, J_i, l_i, a_i, b_i indicate the mass, moment of inertia, pendulum link length, the relative position of the pendulum link center of gravity and friction of the i-th joint or link, where $i = 0, \dots, n$, parameter g is the gravitational acceleration. Force actuating the cart is here denoted $f(t)$. We will assume that the virtual action variable is the cart acceleration (i.e. the reverse action of the pendulum on the cart is omitted). In other words, we can say that the cart will be driven by the ideal velocity controller. Since the system will be affected by nonconservative viscous friction forces we need to further form the Rayleigh dissipation function which holds as follows

$$D(t) = \frac{1}{2} b_1 \left(\frac{d\theta_1(t)}{dt} \right)^2 + \sum_{k=2}^{n} \frac{1}{2} b_k \left[\left(\frac{d\theta_k(t)}{dt} \right) - \left(\frac{d\theta_{k-1}(t)}{dt} \right) \right]^2 + \frac{1}{2} b_0 \left(\frac{dy_0(t)}{dt} \right)^2. \tag{6}$$

Now, we will define the generalized coordinates of the pendulum model as

$$[q_1(t), \dots, q_{n+1}(t)]^T = [\theta_1(t), \dots, \theta_n(t), y_0(t)]^T \tag{7}$$

and the equations of motion for n-link pendulum on a cart model can be written as

$$\frac{d}{dt} \left(\frac{\partial L(t)}{\partial \dot{q}_k(t)} \right) - \frac{\partial L(t)}{\partial q_k(t)} + \frac{\partial D(t)}{\partial \dot{q}_k(t)} = 0, \quad k = 1, \dots, n, \tag{8}$$

$$\frac{d}{dt} \left(\frac{\partial L(t)}{\partial \dot{q}_{n+1}(t)} \right) - \frac{\partial L(t)}{\partial q_{n+1}(t)} + \frac{\partial D(t)}{\partial \dot{q}_{n+1}(t)} = f(t) \tag{9}$$

where $L(t) = T(t) - V(t)$ is called Lagrangian.

Now, by evaluating equations (8), (9) for $n = 2$ and assuming that the cart is driven by the ideal velocity controller, we acquire the nonlinear motion equations for a double pendulum on a cart

$$p_1 \ddot{\theta}_1(t) + p_2(-gsin(\theta_1(t)) + u(t)cos(\theta_1(t))) + p_3 \dot{\theta}_1(t) + p_4(\dot{\theta}_1(t) - \dot{\theta}_2(t)) = -\ddot{\theta}_2(t)cos(\theta_1(t) - \theta_2(t)) - \dot{\theta}_2^2(t)sin(\theta_1(t) - \theta_2(t)), \tag{10}$$

$$p_5 \ddot{\theta}_2(t) + p_6(-gsin(\theta_2(t)) + u(t)cos(\theta_2(t))) + p_4(\dot{\theta}_2(t) - \dot{\theta}_1(t)) = -\ddot{\theta}_1(t)cos(\theta_2(t) - \theta_1(t)) - \dot{\theta}_1^2(t)sin(\theta_2(t) - \theta_1(t)), \tag{11}$$

$$\ddot{y}_0(t) = u(t) \tag{12}$$

with parameters

$$p_1 = \frac{m_1 a_1^2 l_1^2 + m_2 l_1^2 + J_1}{m_2 l_1 a_2 l_2}, \quad p_2 = \frac{m_1 a_1 l_1 + m_2 l_1}{m_2 l_1 a_2 l_2}, \quad p_3 = \frac{b_1}{m_2 l_1 a_2 l_2}, \quad p_4 = \frac{b_2}{m_2 l_1 a_2 l_2}, \quad p_5 = \frac{m_2 a_2^2 l_2^2 + J_2}{m_2 l_1 a_2 l_2}, \quad p_6 = \frac{1}{l_1}. \tag{13}$$

We can transform the system to the state-space realization and linearize it around the lower stable equilibrium point resulting in a model

$$\dot{\vec{x}}(t) = \mathbf{A}\vec{x}(t) + \vec{b}u(t), \tag{14}$$

where $\vec{x}(t) = [\theta_1(t) - \pi, \theta_2(t) - \pi, y_0(t), \dot{\theta}_1(t), \dot{\theta}_2(t), \dot{y}_0(t)]^T$ and

$$\mathbf{A} = \begin{bmatrix} 0 & 0 & 0 & 1 & 0 & 0 \\ 0 & 0 & 0 & 0 & 1 & 0 \\ 0 & 0 & 0 & 0 & 0 & 1 \\ \frac{p_2 p_5 g}{1 - p_1 p_5} & -\frac{p_6 g}{1 - p_1 p_5} & 0 & \frac{p_4 + p_3 p_5 + p_4 p_5}{1 - p_1 p_5} & -\frac{p_4 + p_4 p_5}{1 - p_1 p_5} & 0 \\ -\frac{p_2 g}{1 - p_1 p_5} & \frac{p_1 p_6 g}{1 - p_1 p_5} & 0 & -\frac{p_3 + p_4 + p_1 p_4}{1 - p_1 p_5} & \frac{p_4 + p_1 p_4}{1 - p_1 p_5} & 0 \\ 0 & 0 & 0 & 0 & 0 & 0 \end{bmatrix}, \tag{15}$$

$$\vec{b} = \left[0, 0, 0, \frac{p_6 - p_2 p_5}{1 - p_1 p_5}, \frac{p_2 - p_1 p_6}{1 - p_1 p_5}, 1 \right]^T. \tag{16}$$

Transfer function model can be subsequently derived for the assumed plant input and output in a general form of

$$P(s) = \frac{\Theta_1(s)}{s^2 Y_0(s)} = \frac{K(s^2 + 2\xi_z \omega_z s + \omega_z^2)}{(s^2 + 2\xi_1 \omega_1 s + \omega_1^2)(s^2 + 2\xi_2 \omega_2 s + \omega_2^2)}, \tag{17}$$

where $\Theta_1(s)$ is the deflection angle of the rope, $s^2 Y_0(s)$ denotes gantry acceleration and the modal parameters ξ_i, ω_i arise as functions of the physical parameters in (13).

B. Load-side motion sensing

Inertial measurement unit equipped with 3-axis accelerometer and gyroscpe is used as a load motion sensor attached to the hook. Sensor fusion algorithm was implemented to improve overall sensing accuracy. A quaternion-based heading estimation method used in [20], [21] was employed leading to a nonlinear state reconstruction problem for the system

$$\underbrace{\begin{bmatrix} \dot{q}_1(t) \\ \dot{q}_2(t) \\ \dot{q}_3(t) \\ \dot{q}_4(t) \end{bmatrix}}_{\vec{q}(t)} = \underbrace{\frac{1}{2} \begin{bmatrix} 0 & -\omega_x(t) & -\omega_y(t) & -\omega_z(t) \\ \omega_x(t) & 0 & \omega_z(t) & -\omega_y(t) \\ \omega_y(t) & -\omega_z(t) & 0 & \omega_x(t) \\ \omega_z(t) & \omega_y(t) & -\omega_x(t) & 0 \end{bmatrix}}_{\mathbf{A}(\vec{\omega}(t))} \underbrace{\begin{bmatrix} q_1(t) \\ q_2(t) \\ q_3(t) \\ q_4(t) \end{bmatrix}}_{\vec{q}(t)}, \tag{18}$$

$$\vec{y}(t) = \begin{bmatrix} g_x(t) \\ g_y(t) \\ g_z(t) \end{bmatrix} = \mathbf{R}(\vec{q}(t)) \begin{bmatrix} 0 \\ 0 \\ -g \end{bmatrix}, \tag{19}$$

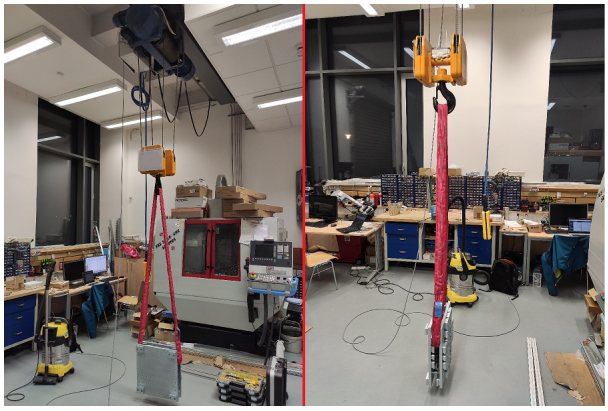

Fig. 2. Five ton industrial gantry crane used for the experiments

with $\vec{q}(t)$ denoting the state vector represented by the unit quaternion containing the information about the hook sway angles with respect to the inertial reference frame and $\omega_x(t)$, $\omega_y(t)$, $\omega_z(t)$ being the hook angular rates in the particular axes. The output $\vec{y}(t)$ then represents the gravitational accelerations expected to be measured in the individual axes by the IMU, $\mathbf{R}(\vec{q}(t))$ is the rotation matrix expressing the same information as $\vec{q}(t)$ and g is the gravitational acceleration magnitude.

Extended Kalman filter (EKF) [22] was employed as a non-linear observer. The acquired instantaneous values of inclination angles and angular rates are sent to a controller base-station using a wire-less transmission system of our own development [23].

C. System identification

Relay feedback is used for the automatic excitation of load oscillatory modes, which is necessary for identification of the plant model. The topic of the relay experiment itself is quite complex and out of scope of the current paper. It will be published soon in a separate study. Data collected from an industrial five ton gantry crane setup (Fig. 2) during such an experiment are shown in Fig. 3. The second resonant mode is poorly observable when examining just the deflection angle estimate. However, the situation becomes better when working with angular rate measurements since the derivative amplifies high frequencies by nature. This suggests the use of measured angular velocity $\dot{\theta}_1(t)$ as a system output in the identification procedure. Measured hoist velocity $v(t)$ is then preferred over the velocity set-point as system input in order to reduce the model order.

With respect to these considerations and the knowledge of system dynamics described above, the model structure was chosen as

$$\frac{s\Theta_1(s)}{V(s)} = \frac{b_4 s^4 + b_3 s^3 + b_2 s^2 + b_1 s + b_0}{s^4 + a_3 s^3 + a_2 s^2 + a_1 s + a_0}, \qquad (20)$$

where $s\Theta_1(s)$ is the measured angular rate, $V(s) \triangleq sY_0(s)$ denotes the gantry velocity and $\vec{\theta} = [b_4 \;\; b_3 \;\; b_2 \;\; b_1 \;\; b_0 \;\; a_3 \;\; a_2 \;\; a_1 \;\; a_0]^T$ are the model parameters to be identified.

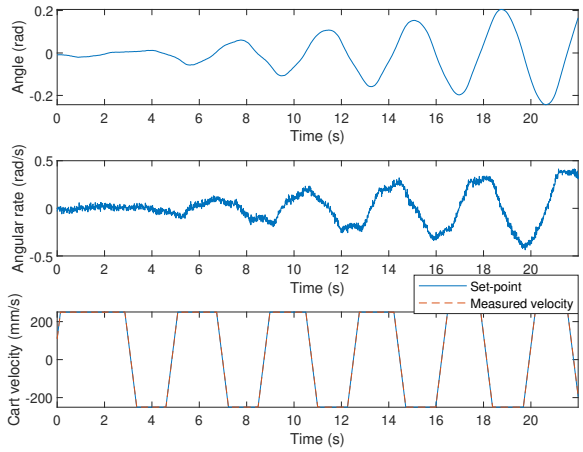

Fig. 3. Measured data as a result of the identification experiment

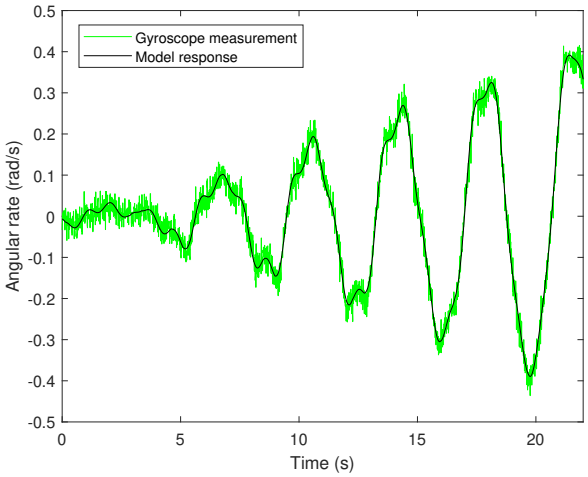

Fig. 4. Response of the model and the measured angular rate

Due to our choice of relay excitation and practical requirement on short experiment duration, we employed time-domain algorithms that do not require steady states and can deal with transient effects well. In particular, the `tfest()` routine of the Matlab System Identification Toolbox was used. This function implements the Simplified Refined Instrumental Variable Method [24] with the subsequent nonlinear least-squares optimization minimizing the weighted prediction error norm.

The following model parameters were obtained

$$\vec{\theta} = \left[\begin{array}{c} -5.88e^{-5}, 1.08e^{-4}, -4.12e^{-3}, -1.75e^{-4}, -3.46e^{-4}, \\ 0.0921, 45.1, 0.51, 127 \end{array} \right]^T. \qquad (21)$$

The model response is plotted in Fig. 4 in comparison with measured data in order to provide a basic model validation. The frequency response is then shown in Fig. 5. The two resonant frequencies correspond to a preliminary frequency

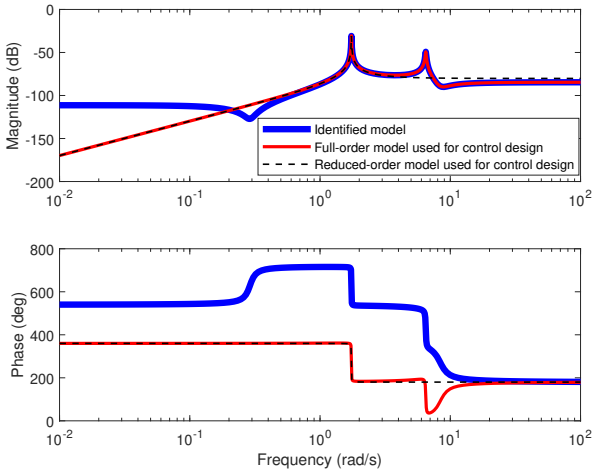

Fig. 5. Model frequency response functions

analysis of the measured data which may be considered as another form of validation.

The identified model (20) contains two resonant modes which is consistent with the physical model (17). However, at low and high frequencies, there is a large difference between both models due to the fact that this deviation contributes little to the estimation error in the time domain. Therefore, the identification may be considered as a first step and the model is then modified for the control system purposes by replacing the low-frequency pair of zeros with two differentiators and by mirroring the high-frequency pair of zeros into the left complex half-plane to reflect the physical nature of the model. The transfer function then has a form

$$\frac{s\Theta_1(s)}{V(s)} = \frac{Ks^2(s^2 + 2\xi_z\omega_z s + \omega_z^2)}{(s^2 + 2\xi_1\omega_1 s + \omega_1^2)(s^2 + 2\xi_2\omega_2 s + \omega_2^2)} \quad (22)$$

with all the model parameters easily determined from (21). Next, a reduced order model was derived by omitting the second resonance and the anti-resonance in (22) resulting in transfer function

$$\frac{s\Theta_1(s)}{V(s)} = \frac{K\frac{\omega_z^2}{\omega_2^2}s^2}{(s^2 + 2\xi_1\omega_1 s + \omega_1^2)}. \quad (23)$$

The corresponding frequency response functions are displayed in Fig. 5.

D. Control strategy

For the active anti-sway control, the algorithm illustrated with Figure 6 was chosen, where $v(t)$ is the cart velocity being the system input, $v_{sp}(t)$ is its set-point and $\theta_1(t)$, $\dot{\theta}_1(t)$ represent the hook angle and angular rate as system outputs. The controlled system is modelled by (22).

First, a full state feedback controller was designed using the reduced-order model (23) to evaluate potential performance deterioration due to the unmodelled dynamics of the second

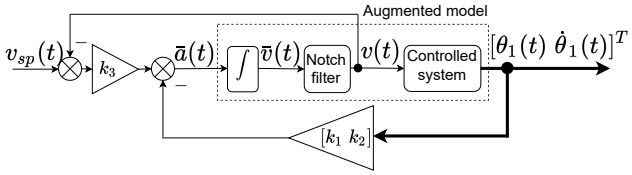

Fig. 6. Control structure diagram

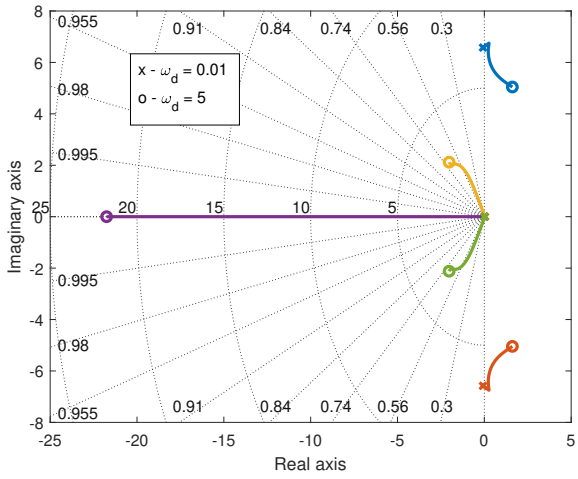

Fig. 7. Root locus without notch filter - full-state feedback for the reduced-order single-mode model

oscillatory mode. The feedback gains k_1, k_2, k_3 were computed by solving the pole-placement problem

$$\det(\mathbf{A}_{\mathbf{aug}}^{\mathbf{red}} - \vec{b}_{aug}^{red}\vec{k}(k_1, k_2, k_3) - \lambda\mathbf{I}) = \prod_{i=1}^{3}(\lambda - p_i) \quad (24)$$

where $\mathbf{A}_{\mathbf{aug}}^{\mathbf{red}}$ and $\vec{b}_{aug}^{red}$ represent the matrix of dynamic and input vector belonging to the state space representation of the augmented model which is denoted by the dashed rectangle in the control diagram.

The desired poles p_i were in all the following cases selected in a Butterworth pattern as $p_1 = -\omega_d$, $p_{2,3} = -0.5\omega_d \pm j\omega_d\sqrt{1-0.5^2}$ with one free design parameter ω_d affecting desired closed-loop bandwidth. The loop was closed with the full-order system (22) to evaluate the mismatch due to unmodelled dynamics. The location of all the closed-loop poles under varrying ω_d parameter was examined. Now, a case without notch filter (i.e. $\bar{v}(t) = v(t)$) is assumed. Figure 7 displays the location of the poles for ω_d ranging from 0.01 to 5. We can notice that the poles that we intended to place directly by the feedback are located elsewhere due to the neglection of the second mode. Next, the poles belonging to the second resonance enter the right half-plane even for small values of ω_d which results in unstable closed-loop dynamics. The performed analysis advocates the modelling effort to find a more complex double-pendulum model capable of properly capturing the second mode dynamics. However, appropriate adjustment of the controller design procedure is also necessary.

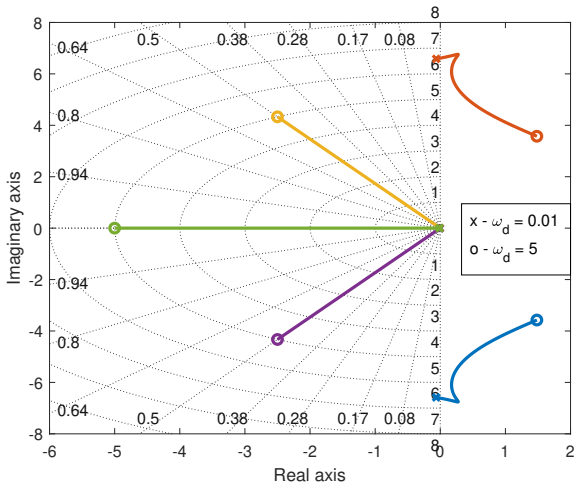

Fig. 8. Root locus without notch filter, $\omega_d \in \langle 0.01; 5 \rangle$

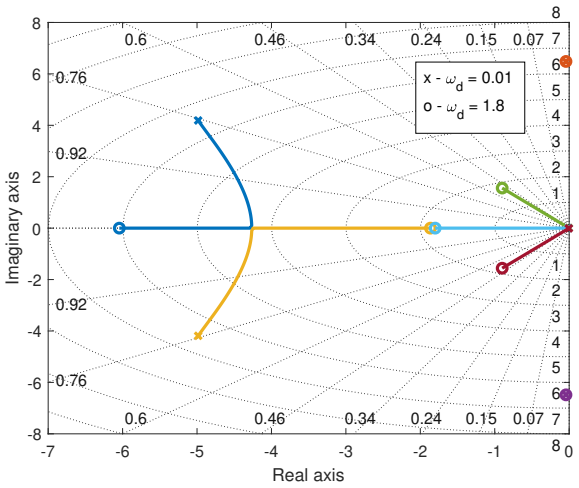

Fig. 9. Root locus with notch filter, $\omega_d \in \langle 0.01; 1.8 \rangle$

The feedback gains k_1, k_2, k_3 may alternatively be found by solving the partial pole placement problem

$$\det(\mathbf{A}_{\mathbf{aug}}^{\mathbf{full}} - \vec{b}_{aug}^{full}\vec{k}(k_1, k_2, k_3) - \lambda\mathbf{I}) = \prod_{i=1}^{3}(\lambda - p_i)\prod_{i=1}^{n-3}(\lambda - p_i^*) \tag{25}$$

where $\mathbf{A}_{\mathbf{aug}}^{\mathbf{full}}$ and $\vec{b}_{aug}^{full}$ belong to the state space representation of the full augmented model of order n. We are clearly able to arbitrarily place three closed-loop poles (denoted as p_i) while the location of the remaining ones (p_i^*) cannot be independently affected. In contrary to the previous design method, this approach advantegeously ensures the precise location of the poles p_1, p_2 and p_3 that were again selected to match the third-order Butterworth polynomial.

First, a case without the notch filter (i.e. $\bar{v}(t) = v(t)$ and $N(s) = 1$) is studied in Fig. 8 showing the location of the closed-loop poles for $\omega_d \in < 0.01, 5 >$. The pair of complex conjugate poles whose location cannot be arbitrarily determined again crosses the imaginary axis even for small values of ω_d which results in unstable closed-loop.

This issue suggests a need to introduce a notch filter for the passive stabilisation of the second resonant mode. A standard notch filter described by transfer function

$$N(s) = \frac{(s^2 + 2\xi_2\omega_2 s + \omega_2^2)}{(s^2 + 2\xi_d\omega_2 s + \omega_2^2)} \tag{26}$$

was chosen, canceling the poles of the second mode and replacing them with sufficiently damped pair of poles with the damping factor set specifically to $\xi_d = 0.8$. Assuming such a control strategy, Figure 9 shows the location of all closed-loop poles for values of ω_d between 0.01 and 1.8. With increasing ω_d, the pair of poles that cannot be directly placed approaches the real axis. One of these poles then proceeds towards the imaginary axis, potentially destabilizing the loop for high values of ω_d. Using this design procedure, there is no risk that the pair of complex conjugate poles that is not directly affected by the designer becomes weakly damped and we can quite simply find a value of ω_d for which a fair closed-loop performance is achieved. It turns out that a reasonable choice is $\omega_d = 1.8$ which is illustrated by Figure 9. It can be observed that for $\omega_d = 1.8$ the pole moving on the real axis towards the right half-plane meets the pole that moves in the other direction and the maximum closed-loop bandwidth is achieved in this way. With further increase of ω_d, the closed-loop bandwidth decreases as this pole approaches the imaginary axis.

III. Experimental Results

The control structure shown in Fig. 6 including the notch filter (26) and using the feedback gains tuned by the partial pole placement method with parameter ω_d set to value 1.8 was then implemented in the REXYGEN real-time control system [25] and experimentally tested on the industrial gantry crane from Fig. 2. In order to verify the relevance of the identified model for the control design purposes as well as the overall viability of the proposed active anti-sway control algorithm in practice, the experimental data were compared with the simulations exploiting the virtual model of the system by means of Fig. 10.

The whole experiment may be divided into two phases. First, the feedback control was inactive and the cart moved according to its inner cart velocity set-point in the form of a rectangular signal leading to oscillatory response of angle and angular velocity. Then, the control algorithm was activated which first resulted in the active damping of the first resonance when the set-point signal was set to 0. Next, when the hoist started to move again, the feedback control caused that the first resonant frequency was no more excited at the cost of slower cart velocity set-point tracking.

Figure 10 shows a good match between the simulation and experimental data which proves the proposed identification and control methodology to be suitable for practical use. A slight difference between real and simulation data may be caused by several factors including the nonlinearity of the real crane

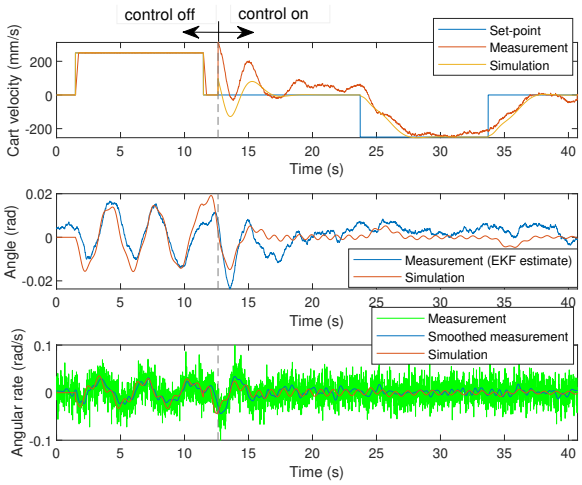

Fig. 10. Experimental results vs simulated closed-loop response

system or neglected reaction forces from the load acting on the gantry. The presence of the inner cart velocity loop which was omitted during the control system design can also play a part as well as possible inaccuracies in sway angle and angular rate measurements.

IV. Conclusion

The paper proposes a feedback control strategy for the active anti-sway system applicable to industrial cranes. The main results of the paper are as follows:

- It is shown that an inertial measurement unit may serve as a suitable sensing device to acquire partial state information.
- The double pendulum model showed to be a relevant representation of the crane dynamics.
- It turns out that proper identification of both oscillatory modes is crucial for the successful employment of the feedback controller.

Future work will deal with the details of the relay identification experiment. We will also focus on the time-variant case considering vertical hoist motions with the attached load which is essential for practical implementation, so that the identification procedure does not have to be repeated whenever the length of the rope changes and so that the control algorithm is robust to model perturbations.

Acknowledgment

This work was supported from ERDF under project "Research and Development of Intelligent Components of Advanced Technologies for the Pilsen Metropolitan Area (InteCom)" No. CZ.02.1.010.00.017_048/0007267.

References

[1] M. Goubej and M. Schlegel, "Feature-based parametrization of input shaping filters with time delays," *IFAC Workshop on time delay systems, Prague*, 2010.

[2] J. Vaughan, D. Kim, and W. Singhose, "Control of tower cranes with double-pendulum payload dynamics," *IEEE Transactions on Control Systems Technology*, vol. 18, no. 6, pp. 1345–1358, 2010.

[3] W. Singhose, D. Kim, and M. Kenison, "Input shaping control of double-pendulum bridge crane oscillations," *Journal of Dynamic Systems, Measurement, and Control*, vol. 130, no. 3, p. 034504, 2008.

[4] M. Giacomelli, F. Padula, L. Simoni, and A. Visioli, "Simplified input-output inversion control of a double pendulum overhead crane for residual oscillations reduction," *Mechatronics*, vol. 56, pp. 37 – 47, 2018.

[5] V. Helma and M. Goubej, "Vibration damping in gantry crane systems: Finite horizon optimal control approach," *24th IEEE Internetional Conference on Emerging Technologies and Factory Automation*, 2019.

[6] J. Vaughan, A. Karajgikar, and W. Singhose, "A study of crane operator performance comparing PD-control and input shaping," in *Proceedings of the 2011 American Control Conference*, June 2011, pp. 545–550.

[7] N. Sun, Y. Fang, H. Chen, and B. He, "Adaptive nonlinear crane control with load hoisting/lowering and unknown parameters: Design and experiments," *IEEE/ASME Transactions on Mechatronics*, vol. 20, no. 5, pp. 2107–2119, 2015.

[8] X. He, W. He, J. Shi, and C. Sun, "Boundary vibration control of variable length crane systems in two-dimensional space with output constraints," *IEEE/ASME Transactions on Mechatronics*, vol. 22, no. 5, pp. 1952–1962, 2017.

[9] L. Ramli, Z. Mohamed, A. M. Abdullahi, H. Jaafar, and I. M. Lazim, "Control strategies for crane systems: A comprehensive review," *Mechanical Systems and Signal Processing*, vol. 95, pp. 1 – 23, 2017.

[10] "SIEMENS SimoCrane sway control," https://mall.industry.siemens.com/mall/cs/cz/Catalog/Products/10218465, accessed: 2020-01-15.

[11] "Smartcrane anti-sway control," www.smartcrane.com, accessed: 2020-01-15.

[12] H. Kawai, Y. B. Kim, and Y. W. Choi, "Anti-sway system with image sensor for container cranes," *Journal of Mechanical Science and Technology*, vol. 23, pp. 2757–2765, 2009.

[13] G. O. Tysse, A. Cibicik, and O. Egeland, "Vision-based control of a knuckle boom crane with online cable length estimation," *IEEE/ASME Transactions on Mechatronics*, 2020.

[14] H. Kawai, Y. Kim, and Y. Choi, "Measurement of a container crane spreader under bad weather conditions by image restoration," *IEEE Transactions on Instrumentation and Measurement*, vol. 61, no. 1, pp. 35–42, 2012.

[15] Y. Kim, Y. Kim, Y. S. Jung, I. G. Jang, K. Kim, S. Kim, and B. M. Kwak, "Developing accurate long-distance 6-dof motion detection with one-dimensional laser sensors: Three-beam detection system," *IEEE Transactions on Industrial Electronics*, vol. 60, no. 8, pp. 3386–3395, 2013.

[16] Y. Kim, K. Hong, and S. Sul, "Anti-sway control of container cranes: Inclinometer, observer, and state feedback," *International Journal of Control, Automation, and Systems*, vol. 2, pp. 435–449, 2004.

[17] V. Kempe, *Inertial MEMS: Principles and Practice*, 1st ed. Cambridge University Press, 2011.

[18] P. A., *Vibration control of active structures*. Springer, 2011.

[19] J. Königsmarková and M. Schlegel, "Identification of n-link inverted pendulum on a cart," in *2017 21st International Conference on Process Control (PC)*, June 2017, pp. 42–47.

[20] M. Řezáč, "Inertial stabilization, estimation and visual servoing for aerial surveillance," Ph.D. dissertation, Czech Technical University in Prague, 2013.

[21] M. Kok, J. D. Hol, and T. B. Schön, "Using inertial sensors for position and orientation estimation," *Foundations and Trends® in Signal Processing*, vol. 11, no. 1-2, pp. 1–153, 2017.

[22] B. P. Gibbs, *Advanced Kalman filtering, least-squares and modeling: a practical handbook*. John Wiley & Sons, 2011.

[23] R. Čečil, V. Šetka, D. Tolar, and A. Sikora, "RETIS – real-time sensitive wireless communication solution for industrial control applications," in *5th International Symposium on Smart and Wireless Systems*, 2020.

[24] P. Young and A. Jakeman, "Refined instrumental variable methods of recursive time-series analysis part III. extensions," *International Journal of Control*, vol. 31, no. 4, pp. 741–764, 1980.

[25] "REXYGEN - programming automation devices without hand coding," www.rexygen.com, accessed: 2020-03-02.